HHS Public Access

Author manuscript

Neurobiol Aging. Author manuscript; available in PMC 2018 October 22.

Published in final edited form as:

Neurobiol Aging. 2018 October ; 70: 160–169. doi:10.1016/j.neurobiolaging.2018.06.016.

Brain regional synchronous activity predicts tauopathy in 3 × TgAD mice

Dong Liu[#a], **Hanbing Lu**[#b], **Elliot Stein**[b], **Zhujuan Zhou**[c], **Yihong Yang**[b], and **Mark P. Mattson**[a,d,*]

[a]Laboratory of Neurosciences, National Institute on Aging Intramural Research Program, Baltimore, MD, USA

[b]Neuroimaging Research Branch, National Institute on Drug Abuse Intramural Research Program, Baltimore, MD, USA

[c]Department of Neurology, Xinqiao Hospital, Army Medical University, Chongquing, China

[d]Department of Neuroscience, Johns Hopkins University School of Medicine, Baltimore MD, USA

[#] These authors contributed equally to this work.

Abstract

Alzheimer's disease (AD) is characterized by progressive cognitive impairment and by extensive neuronal loss associated with extracellular amyloid β-peptide (Aβ) plaques and intraneuronal tau pathology in temporal and parietal lobes. AD patients are at increased risk for epileptic seizures, and data from experimental models of AD suggest that aberrant neuronal network activity occurs early in the disease process before cognitive deficits and neuronal degeneration. The contributions of Aβ and/or tau pathologies to dysregulation of neuronal network activity are unclear. Using a transgenic mouse model of AD (3 × TgAD mice) in which there occurs differential age-dependent development of tau and Aβ plaque pathologies, we applied analysis of resting state functional magnetic resonance imaging regional homogeneity, a measure of local synchronous activity, to discriminate the effects of Aβ and tau on neuronal network activity throughout the brain. Compared to age-matched wild-type mice, 6- to 8-month-old 3 × TgAD mice exhibited increased regional homogeneity in the hippocampus and parietal and temporal cortices, regions with tau pathology but not Aβ pathology at this age. By 18–24 months of age, 3 × TgAD mice exhibited extensive tau and Aβ pathologies involving the hippocampus and multiple functionally related brain regions, with a spatial expansion of increased local synchronous activity to include those regions. Our findings demonstrate that age-related brain regional hypersynchronous activity is associated with early tau pathology in a mouse model, consistent with a role for early tau pathology in the neuronal circuit hyperexcitability that is believed to precede and contribute to neuronal degeneration in AD.

[*]Corresponding author at: National Institute on Aging, Laboratory of Neurosciences, 251 Bayview Blvd Suite 100 Rm 5C214, Baltimore, MD 21224, USA. Tel.: +14105588482; fax: 1 4105588465.

Disclosure statement

The authors have no actual or potential conflicts of interest.

Keywords

Alzheimer's disease; Functional MRI; Hyperexcitability; Hippocampus; Tau; Amyloid beta peptide

1. Introduction

Alzheimer's disease (AD) is characterized by progressive impairment of short-term memory, with most patients also exhibiting behavioral changes including heightened anxiety and agitation (Kelley and Petersen, 2007). These clinical signs in AD patients are, upon postmortem examination, associated with synapse loss and neuronal degeneration in brain regions known to play fundamental roles in learning and memory including the entorhinal cortex, hippocampus (Hip), and parietal and frontal lobes (Coleman and Flood, 1987; Scheff and Price, 2003). These brain regions exhibit prominent, albeit variable, accumulations of extracellular deposits (plaques) of the amyloid β-peptide (Aβ) and intraneuronal accumulation of hyperphosphorylated tau aggregates (Jellinger and Bancher, 1998; Nelson et al., 2009). However, by the time clinical manifestations of AD become apparent, there is extensive Aβ plaque and tau pathology and neuronal loss, making it difficult to understand the relative contributions of these pathological lesions to neuronal network dysfunction and neuronal degeneration that might be applied for therapeutic intervention before clinical manifestation. Advances in the molecular genetics of AD and related dementias have established that mutations in the β-amyloid precursor protein (APP) and presenilin 1 (an enzyme that cleaves APP to generate Aβ) cause rare cases of autosomal dominant familial AD (Bertram et al., 2010; Schellenberg and Montine, 2012), and that tau mutations cause some cases of frontotemporal lobe dementia (Rademakers et al., 2012). Although the associations of Aβ and tau pathologies with neuronal degeneration are generally strong, and pathogenic forms of Aβ and Tau can cause synaptic dysfunction and neuronal degeneration in some experimental models (Brunden et al., 2008; Hochgräfe et al., 2013; Mattson, 2004; Sykora et al., 2015), the events that precede the structural deterioration of neuronal networks have not been established.

Converging evidence from studies of aging (the major risk factor for AD), AD patients and preclinical models suggest that dysregulation of neuronal excitability occurs early in the disease process (Mattson and Arumugam, 2018). Electrophysiological analyses reveal increased excitability of hippocampal and cortical neurons in aged rodents, particularly those that perform more poorly in learning and memory tests (Haberman et al., 2017; Simkin et al., 2015). AD patients, including those with familial AD, are at increased risk for epileptic seizures, and recent findings suggest a very high incidence of sub-clinical epileptiform activity in AD (Born, 2015). Data from longitudinal human studies suggest that neuronal hyperexcitability occurs before cognitive impairment (Cretin et al., 2016). Early cell culture studies demonstrated that pathogenic forms of Aβ (Mattson et al., 1992) and tau (Furukawa et al., 2003) perturb neuronal calcium homeostasis, which can render neurons vulnerable to excitotoxicity, while subsequent studies showed that neurons in transgenic mice that express AD-causing APP, presenilin 1, or tau mutations exhibit vulnerability to excitotoxicity (Decker et al., 2016; Guo et al.,1999; Hall et al., 2015; Palop et al., 2007). However, the

relative contributions of tau and Aβ pathologies to aberrant local neuronal network activity that precedes neuronal death in AD are unclear.

To determine the potential differential impacts of tau and Aβ pathologies on brain regional network function, we used resting state functional magnetic resonance imaging (fMRI) (rs-fMRI) on 3 × TgAD transgenic mice that exhibit early tau pathology and delayed Aβ plaque accumulation, thereby enabling us to discern associations of tau and Aβ pathologies on neuronal network activity throughout the brain. From the rs-fMRI data, we quantified regional homogeneity (ReHo), a voxel-based measure of neuronal network activity that quantifies the synchronization between the time series of a given voxel and its nearest neighbors (Zang et al., 2004). We reasoned that such a change in local neuronal integration would be one manifestation of the observed dysregulation of neuronal excitability. Compared to age-matched wild-type (WT) mice, young 3 × TgAD mice exhibited significantly increased ReHo activity in Hip and associated temporal and parietal lobe structures that also exhibited tau, but not Aβ pathology. Aged 3 × TgAD mice exhibited extensive tau and Aβ pathologies involving Hip and multiple functionally related brain regions, and these same brain regions exhibited increased ReHo. Our findings demonstrate that early accumulation of tau in neurons is associated with elevated resting state synchronous neuronal circuit activity in the Hip and functionally associated brain regions implicated in AD pathogenesis and suggest a therapeutic potential for early, presymptomatic interventions that inhibit tau accumulation and/or normalize neuronal network activity. Because identical rs-fMRI signals can be obtained from both preclinical models and humans, findings from this imaging technique are readily translated to clinical applications.

2. Materials and methods

2.1. Mice

The generation and characterization of the initial line of 3 × TgAD mice was reported previously (Oddo et al., 2003). The mice express mutant human presenilin 1 (M146V) under the control of the endogenous presenilin 1 promoter (Guo et al., 1999) and mutant human APP (Swedish mutation) and mutant tau (P301L mutation; Schoch et al., 2016) both under the control of a Thy 1.2 promoter. The initial 3 × TgAD mice were crossbred to C57BL/6 mice for 8 generations, and this congenic line has been characterized in previous studies (Halagappa et al., 2007; Liu et al., 2010; Romberg et al., 2011). Breeding colonies of WT C57BL/6 and 3 × TgAD mice were maintained in the National Institute on Aging Intramural Research Program vivarium. Genotyping confirmed the presence of mutant genes by reverse transcriptase polymerase chain reaction on each 3 × TgAD mouse used. The mice were housed 3–4 per cage with ad libitum access to food and water in a room with a reverse 12-hour light/12-hour dark cycle with lights on at 18:00 hours. WT and 3 × TgAD mice of two different age groups (6–8 months old and 18–24 months old) were studied (n = 8–10/group). All procedures using live mice were approved by the National Institute on Aging Animal Care and Use Committee and complied with National Institutes of Health guidelines.

2.2. Functional magnetic resonance brain imaging

Mice were imaged while lightly anesthetized using a combination of a low concentration of isoflurane and the α-adrenoreceptor agonist dexmedetomidine (Zoetis, Parisippany, NJ, USA) as previously developed for rat fMRI (Lu et al., 2012). Mice were initially anesthetized with 2% isoflurane in an anesthesia induction chamber, and then administered an i.p. injection of 0.015 mg/kg dexmedetomidine. Mice were then placed in a customized animal holder in a prone position with their heads secured with a custom-made bite bar and ear bars. A custom-made nose cone was used to deliver isoflurane mixed in oxygen-enriched air, and exhaled gas was removed from the nose cone using a vacuum line. The flow rate of the vacuum line was monitored and maintained at the same level across animals. The respiration rate was monitored continuously using a pneumatic sensor (SA instrument Inc, New York, USA). The body temperature was measured with a rectal probe (CWE, Inc, PA, USA) and maintained at 37.5 ± 0.5 °C using a water-circulating heating pump. The fur on the lower back of the animal was shaved, and continuous subcutaneous infusion of dexmedetomidine (0.015 mg/kg/h) was administered via a needle attached to PE30 tubing. Isoflurane was delivered via a calibrated vaporizer initially at a concentration of 1.5%−2%, while animals were secured within the cradle and moved into the center of the magnet, and was gradually reduced to and maintained at 0.5%−0.75% throughout fMRI data acquisition. fMRI data were acquired beginning approximately 90 minutes after anesthesia induction using a Bruker Biospin 9.4 T scanner operating on a ParaVision 6.0.1 platform (Bruker Medizintechnik, Karlsruhe, Germany) with an active-shielded gradient coil capable of generating a 400 mT/m gradient field. Radio frequency excitation was applied with a quadrature volume transmit coil (86 mm ID), and a single-turn surface coil (2 cm) was used for magnetic resonance signal reception. High-resolution T_2-weighted brain images were acquired using a rapid acquisition with relaxation enhancement sequence. Scan parameters were repetition time = 2500 ms, effective echo time = 40 ms, rapid acquisition with relaxation enhancement factor = 8, field of view = 2.5 × 2.5 cm^2, matrix size = 256 × 256. Twenty-five slices of brain were acquired with a slice thickness of 0.6 mm. The decussation of the anterior commissure (approximately 0.0 mm from bregma) served as a fiducial landmark to standardize slice localization both within and across mice. Functional images were acquired using a single-shot gradient echo echo-planar imaging (EPI) sequence. Scan parameters were field of view = 2.5 × 2.5 cm^2; matrix size = 64 × 64; repetition time = 1200 ms; echo time = 15 ms; number of slices = 15; slice thickness = 0.6 mm; data acquisition bandwidth 250 kHz; number of repetition = 300. Each resting scan session lasts for 6 minutes.

2.3. fMRI data analysis

rs-fMRI data were processed using analysis of functional neuro-images (AFNI) (Cox, 2012) software platform. MRI data from individual mice were coregistered into a common space in three steps. First, high-resolution anatomical images were skull-stripped, with anatomical and functional images from one mouse that had the best positioning chosen as the template. High-resolution anatomical images from all other mice were then coregistered to the template using the 3dAllineate function in AFNI; the same transformation matrix was applied to EPI images. Second, registered EPI images from all rats were averaged, generating a group average EPI template. Finally, EPI images from all mice were

coregistered to the EPI template using the 3dAllineate function. fMRI data preprocessing steps included denoising using independent component analysis (ICA), slice-timing correction, linear and quadratic trend removal and spatial smoothing with a Gaussian kernel (full width at half maximum = 0.6 mm).ICA denoising was performed using the MELODIC software package in FSL (Oxford University, UK). Data were then band-pass filtered between 0.01 and 0.1 Hz. The time courses from 11 white matter voxels were averaged to represent the white matter signal, and fourteen voxels from the lateral ventricle were averaged to represent cerebral spinal fluid signal. These two measures were considered nuisance signals related to physiological noise (mostly from respiration and cardiac pulsation) and were regressed out using the 3dDeconvolve function in AFNI.

ReHo reflects the synchrony of the spontaneous blood oxygen level dependent (BOLD) fluctuations of individual voxels with all neighboring voxels, such that a higher ReHo value indicates a greater regional synchrony in BOLD fluctuations (Zang et al., 2004). ReHo was computed on a voxel-wise basis using the AFNI program 3dReHo; the number of neighboring voxels was set to 7 to accommodate the small size of the mouse brain. Thus, for a given voxel, ReHo was calculated by computing the synchrony of the spontaneous BOLD fluctuations of that voxel with its immediate neighboring 6 voxels. ReHo data were subjected to statistical comparisons between groups using the AFNI program 3dMVM (between-subjects fixed factors; 3 × TgAD vs. WT × young vs. old).The AFNI program 3dClustSim was used to estimate the probability of false positive clusters and was used to set a statistical threshold accounting for multiple comparisons. A corrected $p < 0.05$ was considered significant throughout and was calculated based on a cluster size of 26 (uncorrected $p < 0.01$). As a secondary procedure, we applied group ICA to identify brain networks. This was done using the MELODIC package in FSL with the number of components specified to be either 15, 20, or 30.

2.4. Immunohistochemistry

Immunohistological analyses were performed on the brains of all mice used for the fMRI analyses using methods similar to those described previously (Liu et al., 2010). Briefly, within 2 days of scanning, mice were anesthetized with isoflurane gas and perfused transcardially with saline, and then 4% paraformaldehyde in phosphate buffered saline (PBS). The brains were removed, postfixed in 4% paraformaldehyde in PBS at 4 °C overnight, and cryoprotected by immersion in PBS containing 20%–30% sucrose at 4 °C for 3 days, then stored at – 80 °C. Brains were sectioned at 20 μm thickness in the coronal plane. For immunostaining, endogenous peroxidases were quenched by immersing sections in a solution of 0.3% hydrogen peroxide in methanol. The sections were then incubated in Tris-buffered saline (TBS) with bovine serum albumin or normal goat serum and 0.2% Triton X-100 in TBS for 1 hour before incubation with primary antibody overnight at 4 °C. The following antibodies were used in this study: anti-Aβ: 6E10 (Covance, Dedham, MA, USA); anti-human tau T13, HT7 (Thermo Fisher Scientific, Waltham, MA, USA); phosphorylated tau AT180 (pT231, Thermo Fisher Scientific), and conformational p-tau Als-50 (generous gift from Dr Peter Davies, at Albert Einstein College of Medicine, New York, USA). After incubation with a primary antibody, sections were incubated for 1 hour in TBS containing at 1:400 dilution of Alexa 488–conjugated secondary antibodies (Abcam,

Cambridge, MA, USA) appropriate for the species of the primary antibody. Confocal images were acquired and processed using a Zeiss LSM510 or LSM 710 microscope system (Carl Zeiss Inc, Jena, Germany). A standard streptavidin-biotin-peroxidase labeling method (Vector ABC kit) and the chromogen 3,3′-diaminobenzidine were used for nonimmunofluorescence staining.

2.5. Quantification of regional tau pathology

Brain regional intensity quantification was performed on brain sections that included the regions of interest. The average density of regional human tau (hTau) immunoreactivity was evaluated on at least 3–4 comparable brain sections/per mouse from 8 mice in each of the 2 age groups of AD mice. The same scanning settings and magnification were applied for image acquisition. The boundaries of each brain region evaluated were established using a mouse brain atlas (Paxinos and Frankline, 2012). For quantification, the images were converted to grayscale and then the average regional pixel intensity of hTau immunoreactivity was determined using ImageJ (National Institutes of Health) software. Data were presented as mean ± standard error of the mean.

2.6. Immunoblot analyses

The immunoblot method was described previously (Liu et al., 2013). Briefly, brain tissues were dissected and homogenized in a protein extraction buffer (Thermo Scientific), plus complete protease inhibitor cocktail tablets and phosphatase inhibitors (Roche Diagnostics, USA). The protein samples were separated on pre-casting gradient gels at 30 μg/lane (Tris-glycine gels, Invitrogen, USA) after protein concentration quantification (BCA kit, Pierce), and transferred to a nitrocellulose membrane, which was blocking with 5% nonfat milk in TBS for 1 hour, then incubated with the primary antibody, followed by the appropriate horse radish peroxidase-conjugated secondary antibody.

The sarkosyl-insoluble tau assay was performed as described previously (Delobel et al., 2008) with minor modifications. Briefly, brain tissue (whole cortical tissue) was homogenized in TBS and centrifuged at 10,000× g for 20 minutes. The supernatant was removed, and the pellet was rehomogenized in Tris buffer with 1% Triton X-100 and ultracentrifuged at100,000× g for 30 minutes at 4 °C. The supernatant was collected as Triton-soluble fraction, and the pellet was incubated with 1% sarkosyl for 30 minutes before ultra-centrifugation again at 100,000× g for 30 minutes. The supernatant was the sarkosyl-soluble fraction, and the pellet was the sarkosyl-insoluble fraction. The sarkosyl-insoluble fraction was then solubilized in a urea buffer. After protein concentration quantification, equal amounts of proteins in the Triton fraction, sarkosyl-soluble, and sarkosyl-insoluble fractions were separated electrophoretically in a 4%−12% sodium dodecyl sulfate polyacrylamide gel electrophoresis, transferred to nitrocellulose membrane, and blotted with antibodies against human-specific tau and phosphorylated tau. Horse radish peroxidase-conjugated secondary antibodies were used in all immunoblots (Vector Laboratories) and were visualized using a chemiluminescence reagent (Pierce, Rockford, IL, USA). The integrated density of protein bands was quantified by densitometric analysis and Image J software (National Institutes of Health) and normalized to the β-actin band density in the same sample.

2.7. Statistics

Two-way analysis of variance was used to assess differences in ReHo values, tau and Aβ pathology density, and two-tailed post hoc *t* test was used for determination of significance between group mean values. For determination of correlations between regional ReHo changes (AD vs. age-matched WT mice) and tauopathy, we used general linear regression analysis. A $p < 0.05$ was considered significant throughout.

3. Results

3.1. Brain regional rs-fMRI analysis reveals age-related increases in ReHo values in Hip and functionally associated cerebral cortical regions in 3 × TgAD mice

We investigated ReHo by rs-fMRI, a measure of local synchrony of spontaneous BOLD fluctuations in a mouse model of AD (3 × TgAD) mice versus age-matched WT mice. ReHo in the Hip, temporal association cortex (TAC), and auditory association cortex (AAC) was significantly greater in young (6–8 months) 3 × TgAD mice compared to young WT mice, suggesting aberrant functional activity of neuronal circuits in these brain regions (Fig. 1A, C). The ReHo in the Hip, Sub, TAC, and AAC of old 3 × TgAD mice (18–24 months of age) mice was significantly greater than age-matched WT mice (Fig. 1B, C). In addition, old 3 × TgAD mice exhibited elevated ReHo in the lateral entorhinal cortex (LEC) and nucleus accumbens (NA). The magnitudes of the elevated ReHo in Hip, LEC, TAC, AAC, and NA in 3 × TgAD versus WT mice were significantly greater in old compared to young mice (Fig. 1C).

3.2. Tau pathology is correlated with aberrant ReHo across brain regions of 6- to 8-month-old 3 × TgAD mice

Previous studies have shown that several lines of mice expressing the P301L hTau mutation in neurons, including 3 × TgAD mice, exhibit age-dependent accumulation of pathological hyper-phosphorylated hTau in neurons in the Hip and anatomically associated regions of the cerebral cortex (Cook et al., 2015; Kashiwaya et al., 2013; Liu et al., 2010; Vossel et al., 2017). We therefore immunostained coronal brain sections from mice used for the fMRI analysis with an antibody that specifically binds to hTau (P301L mutant hTau in 3 × TgAD mice) or with an Aβ antibody to determine the potential contributions of these two neuropatho-logical AD features to brain regional synchronous activity indicated by ReHo. In young 3 × TgAD mice, hTau accumulation was prominent in the cell bodies and neurites of neurons in the Hip, Sub, TAC, and hTau-positive neurons in the LEC (Fig. 2A–D). In the 6- to 8-month-old 3 × TgAD mice, the only brain region that exhibited an elevated ReHo and Aβ pathology was the Sub, where neurons exhibited intraneuronal Aβ immunoreactivity but no extracellular plaques were evident (Fig. 2E, F). Quantitative analysis demonstrated a significant positive correlation between differences in ReHo values (AD vs. WT) and hTau immunoreactivity intensity of the brain regions examined (Fig. 2G, H).

3.3. Tau pathology is correlated with elevated ReHo across brain regions of 18- to 24-month-old 3 × TgAD mice

In old × 3 TgAD mice, hTau pathology was extensive within hippocampal CA1 pyramidal neurons and to a lesser extent in dentate granule neurons (Fig. 3A, B). Cortical neurons with hTau pathology were prominent in the TAC and retrosplenial cortex (RSC) (Fig. 3C and D). Aβ pathology was prominent in the Hip, Sub, and RSC (Fig. 3E–H). There was a significant correlation between ReHo value changes (AD vs. WT mice) and hTau immunoreactivity intensity among the brain regions examined in the old 3 × TgAD mice (Fig. 3I and J).

3.4. Biochemical characterization of tauopathy in 3 × TgAD mice

To determine whether the human TauP301L mutant expressed in 3 × TgAD mice recognized by hTau-specific antibody were pathological species of tau (Nobuhara et al., 2017), we evaluated the solubility, aggregation, and phosphorylation of tau in brain samples from 1-year-old 3 × TgAD and WT mice. Samples from 3 × TgAD mice, but not WT mice, contained abundant sarkosyl-insoluble tau, which was detected with an antibody specific for hTau and an antibody that recognizes hyperphosphorylated tau (Alz50) (Fig. 4A). When normalized to β-actin levels, the amounts of sarkosyl-insoluble tau were greater than levels of sarkosyl-soluble tau (Fig. 4B). The hTau proteins recognized by hTau antibody include two major bands at 55 kDa and 64 kDa. The high molecular weight band at 64 kDa is likely the hyperphosphorylated aggregation-prone tau species (Sahara et al., 2002) and was only detectable in sarkosyl-insoluble fraction from AD mice. Standard immunoblotting showed that hTau protein was present in brain samples from AD mice and was not detectable in samples from WT mice (Fig. 4C and D). We also immunostained brain sections from 3 × TgAD mice with the hTau-specific antibody, antibody Alz50 which recognizes a human conformational *p*-tau epitope, and AT180 which recognizes a pathological tau that is phosphorylated on threonine 231 (Goedert et al., 1994). There was abundant AT180 immunoreactive staining in hippocampal CA1 neurons and in cerebral cortical neurons with all three tau antibodies (Fig. 4E–H).

4. Discussion

Emerging findings suggest that dysregulation of neuronal network activity precedes and may contribute mechanistically to the degeneration of neurons in vulnerable brain regions in AD (Hall et al., 2015; Palop et al., 2007). In addition to increased incidence of seizures in AD patients (Vossel et al., 2017), a recent study revealed subclinical hippocampal seizures and spikes during sleep in AD patients (Lam et al., 2017). Studies of AD mouse models with cerebral Aβ and/or tau pathologies have demonstrated increased incidence of spontaneous or induced seizures, EEG evidence of global seizure-like activity, and increased excitability of hippocampal and entorhinal cortex projection neurons measured using intracellular electrodes (García-Cabrero et al., 2013; Kam et al., 2016; Kazim et al., 2017). Our rsfMRI ReHo analysis, a measure of local synchronous network activity (Zang et al., 2004), in a mouse model that develops progressive accrual of tau and Aβ pathologies (Halagappa et al., 2007; Liu et al., 2010; Romberg et al., 2011), provides three novel advances beyond previous studies of Aβ, tau, and neuronal excitability in AD. First, we found a progressive increase in the ReHo of local neuronal circuits in the Hip and several of its functionally

connected cortical structures. Second, we describe age-dependent expansion of brain regions exhibiting elevated synchronous activity. Third, we demonstrate that early (young, 6–8 months) aberrant brain regional activity assessed by ReHo analysis is mostly associated with tau neuropathology in the absence of apparent Aβ pathology in 3 × TgAD mice. In young 3 × TgAD mice, Aβ accumulation was only apparent intracellularly in neuron in the subiculum, whereas tau pathology was evident not only in the subiculum but also in hippocampal neurons and neurons in the RSC and TAC. In old 3 × TgAD mice, tau pathology had expanded within and across cortical brain regions with a corresponding intensification and expansion of hypersynchronous activity in those brain regions. The accumulation of Aβ pathology may also contribute to the increase in brain regional hypersynchronous activity that occurred between young and old age. However, because our tau and Aβ immunoreactivity data were derived from an anatomical region of interest, while the ReHo values were functionally defined from the rs-fMRI images, it should be emphasized that they are not derived from an exact overlap of the same tissue and thus do not provide sufficient resolution to determine whether particular neuronal circuits within the brain region are differentially affected by tau and/or Aβ pathologies.

The Hip is consistently heavily affected by tau pathology and neuronal degeneration in AD, and damage to neurons in this brain region is likely responsible for the early clinical symptoms in AD, namely impaired short-term memory (Markesbery, 2010). Our rs-fMRI ReHo analysis suggests that hippocampal neuronal networks exhibit hypersynchronous activity early in 3 × TgAD mice, and that brain regions functionally connected to the Hip and known to be affected in AD patients (LEC, Sub, TAC, AAC, and RSC) exhibit concomitant or subsequent hypersynchronous activity. The hypersynchronous activity in the Hip and functionally connected brain regions was associated strongly with tau pathology. In contrast, the striatum, a brain minimally affected in AD patients and devoid of tau pathology in 3 × TgAD mice, did not exhibit hyper-synchronous activity. Interestingly, our fMRI analysis revealed increased ReHo in the NA of old 3 × TgAD mice compared to young 3 × TgAD mice. While not typically considered a vulnerable brain region in AD, tau pathology has been documented in the NA of dementia patients with tau tangle-predominant pathology (Kawakami et al., 2014). Moreover, patients with frontotemporal dementia, a disease with extensive tau tangle pathology but devoid of Aβ pathology, exhibit behavioral abnormalities associated with the NA including apathy and disinhibition (Zamboni et al., 2008).

The cellular and molecular mechanisms by which neuronal network activity becomes dysregulated in AD have not been established. Early studies showed that aggregating Aβ can increase neuronal vulnerability to excitotoxicity by inducing membrane lipid peroxidation which, in turn, impairs the function of membrane ion-motive ATPases (Na^+/K^+-ATPase and Ca^{2+}-ATPase) and the neuronal glucose transporter GLUT3 (Mark et al., 1995a,b; Keller et al., 1997). Aβ and tau may also increase neuronal excitability by impairing K^+ channel function (Hall et al., 2015). Tau may itself contribute to abnormal neuronal excitability because genetic deletion or knockdown of tau can protect neurons against excitotoxicity (DeVos et al., 2013; Holth et al., 2013). Consistent with the latter findings, patients with frontotemporal dementia caused by an inherited tau mutation often exhibit epileptic seizures (García-Cabrero et al., 2013); such patients exhibit robust tau pathology with little or no Aβ pathology (Dermaut et al., 2005). While intraneuronal accumulation of tau pathology and

extracellular aggregation of Aβ may alter neuronal excitability and thereby contribute to synaptic dysfunction and neuronal death, there is also evidence that dysregulation of neuronal excitability can trigger tau and Aβ pathologies. Overactivation of glutamate receptors can induce pathogenic tau accumulation in hippocampal neurons in culture and in vivo by a mechanism involving excessive Ca^{2+} influx (Elliott et al., 1993; Mattson, 1990; Mairet-Coello et al., 2013; Zempel et al., 2010). Aberrant neuronal network activity can also increase neuronal production of pathogenic forms of Aβ (Yamamoto et al., 2015).

Aberrant local synchronous activity may result from impaired inhibitory (GABAergic) tone within local neuronal circuits. Such a possibility is consistent with data suggesting that impaired GABAergic neurotransmission occurs early in AD and with data from animal studies of AD mouse models demonstrating beneficial effects of GABAergic agonists on cognition (Calvo-Flores et al., 2018). Our ReHo analyses revealed increased synchronous activity in the temporal cortex and AAC, brain regions known to be affected in AD. These brain regions provide input to the entorhinal cortex and Hip, two brain regions heavily affected in AD. However, our findings do not reveal whether aberrant neuronal network activity in these brain regions contributes to pathology in the entorhinal cortex and Hip. Previous studies have demonstrated disruptions in functional connectivity between brain regions in patients with AD or mild cognitive impairment compared to age-matched control subjects. In particular, reduced connectivity between neuronal circuits in the default mode network and brain regions involved in cognition have been widely reported (Dennis and Thompson, 2014; Sheline and Raichle, 2013). Our findings reveal that, at least in the 3 × TgAD mouse model, aberrant synchronous neuronal network activity occurs in brain regions affected by tau pathology. When taken together with the data from studies of AD patients, our findings therefore suggest an association between dysregulation of neuronal excitability within brain regions and functional disconnection of those brain regions with other brain regions critical for cognition.

In summary, our data demonstrate that regional hyper-synchronous activity is associated with tau pathology at an early age in a mouse model of AD. These findings suggest that interventions that constrain neuronal excitability within normal limits may have therapeutic efficacy in AD patients. Previous studies have shown that anticonvulsant drugs (Mark et al., 1995b) and a ketone ester (Kashiwaya et al., 2013) can mitigate Aβ and tau pathologies and protect neurons against degeneration in experimental models of AD. Anticonvulsants are prescribed to AD patients with seizures (Vossel et al., 2017), and preclinical studies in AD animal models suggest that interventions that suppress neuronal hyperexcitability also have potential for slowing the neurodegenerative process and cognitive decline (Kashiwaya et al., 2013; Liu et al., 2010; Qing et al., 2008; Sanchez et al., 2012). Abnormal synchronous activity of neuronal circuits prone to tau pathology discerned by ReHo may provide a new diagnostic tool and a means for monitoring disease progression and treatment responses of patients with cognitive impairment.

Acknowledgements

This research was supported by the Intramural Research Programs of the National Institute on Aging (NIA) and National Institute on Drug Abuse (NIDA). The authors are grateful to F. Indig, C. Moad, S. Camandola, and M.

Wilson at the NIA, and Y. Zhang at NIDA for advice and technical support. The authors also thank P. Davies at the Albert Einstein College of Medicine, New York for providing Alz50 antibody.

This research was supported by the Intramural Research Programs of the National Institute on Aging and the National Institute on Drug Abuse.

References

Bertram L, Lill CM, Tanzi RE, 2010 The genetics of Alzheimer disease: back to the future. Neuron 68, 270–281. [PubMed: 20955934]

Born HA, 2015 Seizures in Alzheimer's disease. Neuroscience 286, 251–263. [PubMed: 25484360]

Brunden KR, Trojanowski JQ, Lee VM, 2008 Evidence that non-fibrillar tau causes pathology linked to neurodegeneration and behavioral impairments.J. Alzheimers Dis 14, 393–399. [PubMed: 18688089]

Calvo-Flores Guzmán B, Vinnakota C, Govindpani K, Waldvogel H, Faull RL, Kwakowsky A, 2018 The GABAergic system as a therapeutic target for Alzheimer'sDisease. J. Neurochem 10.1111/jnc.14345 [Epub ahead of print].

Coleman PD, Flood DG, 1987 Neuron numbers and dendritic extent in normal aging and Alzheimer's disease. Neurobiol. Aging 8, 521–545. [PubMed: 3323927]

Cook C, Kang SS, Carlomagno Y, Lin WL, Yue M, Kurti A, Shinohara M, Jansen-West K, Perkerson E, Castanedes-Casey M, Rousseau L, Phillips V, Bu G, Dickson DW, Petrucelli L, Fryer JD, 2015 Tau deposition drives neuropathological, inflammatory and behavioral abnormalities independently of neuronal loss in a novel mouse model. Hum. Mol. Genet 24, 6198–6212. [PubMed: 26276810]

Cox RW, 2012 AFNI: what a long strange trip it's been. Neuroimage 62, 743–747. [PubMed: 21889996]

Cretin B, Sellal F, Philippi N, Bousiges O, Di Bitonto L, Martin-Hunyadi C, Blanc F, 2016 Epileptic prodromal Alzheimer's disease, a retrospective study of 13 new cases: expanding the spectrum of Alzheimer's disease to an epileptic variant? J. Alzheimers Dis 52, 1125–1133. [PubMed: 27104892]

Decker JM, Krüger L, Sydow A, Dennissen FJ, Siskova Z, Mandelkow E, Mandelkow EM, 2016 The Tau/A152T mutation, a risk factor for frontotemporal-spectrum disorders, leads to NR2B receptor-mediated excitotoxicity. EMBO Rep 17, 552–569. [PubMed: 26931569]

Delobel P, Lavenir I, Fraser G, Ingram E, Holzer M, Ghetti B, Spillantini MG, Crowther RA, Goedert M, 2008 Analysis of tau phosphorylation and truncation in a mouse model of human tauopathy. Am. J. Pathol 172, 123–131. [PubMed: 18079436]

Dennis EL, Thompson PM, 2014 Functional brain connectivity using fMRI in aging and Alzheimer's disease. Neuropsychol. Rev 24, 49–62. [PubMed: 24562737]

Dermaut B, Kumar-Singh S, Rademakers R, Theuns J, Cruts M, Van Broeckhoven C, 2005 Tau is central in the genetic Alzheimer-frontotemporal dementia spectrum. Trends Genet. 21, 664–672. [PubMed: 16221505]

DeVos SL, Goncharoff DK, Chen G, Kebodeaux CS, Yamada K, Stewart FR, Schuler DR, Maloney SE, Wozniak DF, Rigo F, Bennett CF, Cirrito JR, Holtzman DM, Miller TM, 2013 Antisense reduction of tau in adult mice protects against seizures. J. Neurosci 33, 12887–12897. [PubMed: 23904623]

Elliott EM, Mattson MP, Vanderklish P, Lynch G, Chang I, Sapolsky RM, 1993 Corticosterone exacerbates kainate-induced alterations in hippocampal tau immunoreactivity and spectrin proteolysis in vivo. J. Neurochem 61, 57–67. [PubMed: 8515288]

Furukawa K, Wang Y, Yao PJ, Fu W, Mattson MP, Itoyama Y, Onodera H, D'Souza I, Poorkaj PH, Bird TD, Schellenberg GD, 2003 Alteration in calcium channel properties is responsible for the neurotoxic action of a familial frontotemporal dementia tau mutation. J. Neurochem 87, 427–436. [PubMed: 14511120]

García-Cabrero AM, Guerrero-López R, Giráldez BG, Llorens-Martín M, Avila J, Serratosa JM, Sánchez MP, 2013 Hyperexcitability and epileptic seizures in a model of frontotemporal dementia. Neurobiol. Dis 58, 200–208. [PubMed: 23774255]

Goedert M, Jakes R, Crowther RA, Cohen P, Vanmechelen E, Vandermeeren M, Cras P, 1994 Epitope mapping of monoclonal antibodies to the paired helical filaments of Alzheimer's disease:

identification of phosphorylation sites in tau protein. Biochem. J 301, 871–877. [PubMed: 7519852]

Guo Q, Fu W, Sopher BL, Miller MW, Ware CB, Martin GM, Mattson MP, 1999 Increased vulnerability of hippocampal neurons to excitotoxic necrosis in presenilin-1 mutant knock-in mice. Nat. Med 5, 101–106. [PubMed: 9883847]

Haberman RP, Koh MT, Gallagher M, 2017 Heightened cortical excitability in aged rodents with memory impairment. Neurobiol. Aging 54, 144–151. [PubMed: 28104309]

Halagappa VK, Guo Z, Pearson M, Matsuoka Y, Cutler RG, Laferla FM, Mattson MP, 2007 Intermittent fasting and caloric restriction ameliorate age-related behavioral deficits in the triple-transgenic mouse model of Alzheimer's disease. Neurobiol. Dis 26, 212–220. [PubMed: 17306982]

Hall AM, Throesch BT, Buckingham SC, Markwardt SJ, Peng Y, Wang Q, Hoffman DA, Roberson ED, 2015 Tau-dependent Kv4.2 depletion and dendritic hyperexcitability in a mouse model of Alzheimer's disease. J. Neurosci 35, 6221–6230. [PubMed: 25878292]

Hochgräfe K, Sydow A, Mandelkow EM, 2013 Regulatable transgenic mouse models of Alzheimer disease: onset, reversibility and spreading of Tau pathology. FEBS J. 280, 4371–4381. [PubMed: 23517246]

Holth JK, Bomben VC, Reed JG, Inoue T, Younkin L, Younkin SG, Pautler RG, Botas J, Noebels JL, 2013 Tau loss attenuates neuronal network hyperexcit-ability in mouse and Drosophila genetic models of epilepsy. J. Neurosci 33, 1651–1659. [PubMed: 23345237]

Jellinger KA, Bancher C, 1998 Neuropathology of Alzheimer's disease: a critical update. J. Neural. Transm. Suppl 54, 77–95. [PubMed: 9850917]

Kam K, Duffy ÁM, Moretto J, LaFrancois JJ, Scharfman HE, 2016 Interictal spikes during sleep are an early defect in the Tg2576 mouse model of β-amyloid neuropathology. Sci. Rep 6, 20119. [PubMed: 26818394]

Kashiwaya Y, Bergman C, Lee JH, Wan R, King MT, Mughal MR, Okun E, Clarke K, Mattson MP, Veech RL, 2013 A ketone ester diet exhibits anxiolytic and cognition-sparing properties, and lessens amyloid and tau pathologies in a mouse model of Alzheimer's disease. Neurobiol. Aging 34, 1530–1539. [PubMed: 23276384]

Kawakami I, Hasegawa M, Arai T, Ikeda K, Oshima K, Niizato K, Aoki N, Omi K, Higashi S, Hosokawa M, Hirayasu Y, Akiyama H, 2014 Tau accumulation in the nucleus accumbens in tangle-predominant dementia. Acta Neuropathol. Commun 2, 40. [PubMed: 24708916]

Kazim SF, Chuang SC, Zhao W, Wong RK, Bianchi R, Iqbal K, 2017 Early-onset network hyperexcitability in presymptomatic Alzheimer's disease transgenic mice is suppressed by passive immunization with anti-human APP/Aβ antibody and by mGluR5 blockade. Front Aging Neurosci. 9, 71. [PubMed: 28392767]

Keller JN, Pang Z, Geddes JW, Begley JG, Germeyer A, Waeg G, Mattson MP, 1997 Impairment of glucose and glutamate transport and induction of mitochondrial oxidative stress and dysfunction in synaptosomes by amyloid beta-peptide: role of the lipid peroxidation product 4-hydroxynonenal. J. Neurochem 69, 273–284. [PubMed: 9202320]

Kelley BJ, Petersen RC, 2007 Alzheimer's disease and mild cognitive impairment. Neurol. Clin 25, 577–609. [PubMed: 17659182]

Lam AD, Deck G, Goldman A, Eskandar EN, Noebels J, Cole AJ, 2017 Silent hippocampal seizures and spikes identified by foramen ovale electrodes in Alzheimer's disease. Nat. Med 23, 678–680. [PubMed: 28459436]

Liu D, Pitta M, Lee JH, Ray B, Lahiri DK, Furukawa K, Mughal M, Jiang H, Villarreal J, Cutler RG, Greig NH, Mattson MP, 2010 The KATP channel activator diazoxide ameliorates amyloid-b and tau pathologies and improves memory in the 3xTgAD mouse model of Alzheimer's disease. J. Alzheimers Dis 22, 443–457. [PubMed: 20847430]

Liu D, Pitta M, Jiang H, Lee JH, Zhang G, Chen X, Kawamoto EM, Mattson MP, 2013 Nicotinamide forestalls pathology and cognitive decline in Alzheimer mice: evidence for improved neuronal bioenergetics and autophagy procession. Neurobiol. Aging 34, 1564–1580. [PubMed: 23273573]

Lu H, Zuo Q, Gu H, Raichle ME, Stein EA, Yang Y, 2012 Rat brains also have a default mode network. Proc. Natl. Acad. Sci. U. S. A 109, 3979–3984. [PubMed: 22355129]

Mairet-Coello G, Courchet J, Pieraut S, Courchet V, Maximov A, Polleux F, 2013 The CAMKK2-AMPK kinase pathway mediates the synaptotoxic effects of Aβ oligomers through Tau phosphorylation. Neuron 78, 94–108. [PubMed: 23583109]

Mark RJ, Hensley K, Butterfield DA, Mattson MP, 1995a Amyloid beta-peptide impairs ion-motive ATPase activities: evidence for a role in loss of neuronal Ca2+ homeostasis and cell death. J. Neurosci 15, 6239–6249. [PubMed: 7666206]

Mark RJ, Ashford JW, Goodman Y, Mattson MP, 1995b Anticonvulsants attenuate amyloid beta-peptide neurotoxicity, Ca2+ deregulation, and cytoskeletal pathology. Neurobiol. Aging 16, 187–198. [PubMed: 7777136]

Markesbery WR, 2010 Neuropathologic alterations in mild cognitive impairment: a review. J. Alzheimers Dis 19, 221–228. [PubMed: 20061641]

Mattson MP, 1990 Antigenic changes similar to those seen in neurofibrillary tangles are elicited by glutamate and Ca2+ influx in cultured hippocampal neurons. Neuron 4, 105–117. [PubMed: 1690014]

Mattson MP, 2004 Pathways towards and away from Alzheimer's disease. Nature 430, 631–639. [PubMed: 15295589]

Mattson MP, Cheng B, Davis D, Bryant K, Lieberburg I, Rydel RE, 1992 beta-Amyloid peptides destabilize calcium homeostasis and render human cortical neurons vulnerable to excitotoxicity. J. Neurosci 12, 376–389. [PubMed: 1346802]

Mattson MP, Arumugam TV, 2018 Hallmarks of brain aging: adaptive and pathological modification by metabolic states. Cell Metab 27, 1176–1190. [PubMed: 29874566]

Nelson PT, Braak H, Markesbery WR, 2009 Neuropathology and cognitive impairment in Alzheimer disease: a complex but coherent relationship. J. Neuropathol. Exp. Neurol 68, 1–14. [PubMed: 19104448]

Nobuhara CK, DeVos SL, Commins C, Wegmann S, Moore BD, Roe AD, Costantino I, Frosch MP, Pitstick R, Carlson GA, Hock C, Nitsch RM, Montrasio F, Grimm J, Cheung AE, Dunah AW, Wittmann M, Bussiere T, Weinreb PH, Hyman BT, Takeda S, 2017 Tau antibody targeting pathological species blocks neuronal uptake and interneuron propagation of tau in vitro. Am. J. Pathol 187, 1399–1412. [PubMed: 28408124]

Oddo SA, Caccamo JD, Shepherd MP, Murphy TE, Golde R, Kayed R, Metherate Mattson MP, Akbari Y, LaFerla FM, 2003 Triple-transgenic model of Alzheimer's disease with plaques and tangles: intracellular Abeta and synaptic dysfunction. Neuron 39, 409–421. [PubMed: 12895417]

Palop JJ, Chin J, Roberson ED, Wang J, Thwin MT, Bien-Ly N, Yoo J, Ho KO, Yu GQ, Kreitzer A, Finkbeiner S, Noebels JL, Mucke L, 2007 Aberrant excitatory neuronal activity and compensatory remodeling of inhibitory hippocampal circuits in mouse models of Alzheimer's disease. Neuron 55, 697–711. [PubMed: 17785178]

Paxinos G, Franklin K, 2012 Paxinos and Franklin's the Mouse Brain in Stereotaxic Coordinates, fourth ed Academic Press, New York, p. 360.

Qing H, He G, Ly PT, Fox CJ, Staufenbiel M, Cai F, Zhang Z, Wei S, Sun X, Chen CH, Zhou W, Wang K, Song W, 2008 Valproic acid inhibits Abeta production, neuritic plaque formation, and behavioral deficits in Alzheimer's disease mouse models. J. Exp. Med 205, 2781–2789. [PubMed: 18955571]

Rademakers R, Neumann M, Mackenzie IR, 2012 Advances in understanding the molecular basis of frontotemporal dementia. Nat. Rev. Neurol 8, 423–434. [PubMed: 22732773]

Romberg C, Mattson MP, Mughal MR, Bussey TJ, Saksida LM, 2011 Impaired attention in the 3xTgAD mouse model of Alzheimer's disease: rescue by donepezil (Aricept). J. Neurosci 31, 3500–3507. [PubMed: 21368062]

Sahara N, Lewis J, DeTure M, McGowan E, Dickson DW, Hutton M, Yen SH, 2002 Assembly of tau in transgenic animals expressing P301L tau: alteration of phosphorylation and solubility. J. Neurochem 83, 1498–1508. [PubMed: 12472903]

Sanchez PE, Zhu L, Verret L, Vossel KA, Orr AG, Cirrito JR, Devidze N, Ho K, Yu GQ, Palop JJ, Mucke L, 2012 Levetiracetam suppresses neuronal network dysfunction and reverses synaptic and cognitive deficits in an Alzheimer's disease model. Proc. Natl. Acad. Sci. U. S. A 109, E2895–E2903. [PubMed: 22869752]

Scheff SW, Price DA, 2003 Synaptic pathology in Alzheimer's disease: a review of ultrastructural studies. Neurobiol. Aging 24, 1029–1046. [PubMed: 14643375]

Schellenberg GD, Montine TJ, 2012 The genetics and neuropathology of Alzheimer's disease. Acta Neuropathol. 124, 305–323. [PubMed: 22618995]

Schoch KM, DeVos SL, Miller RL, Chun SJ, Norrbom M, Wozniak DF, Dawson HN, Bennett CF, Rigo F, Miller TM, 2016 Increased 4R-tau induces pathological changes in a human-tau mouse model. Neuron 90, 941–947. [PubMed: 27210553]

Sheline YI, Raichle ME, 2013 Resting state functional connectivity in preclinical Alzheimer'sdisease. Biol. Psychiatry 74, 340–347. [PubMed: 23290495]

Simkin D, Hattori S, Ybarra N, Musial TF, Buss EW, Richter H, Oh MM, Nicholson DA, Disterhoft JF, 2015 Aging-related hyperexcitability in CA3 pyramidal neurons is mediated by enhanced a-type K+ channel function and expression. J. Neurosci 35, 13206–13218. [PubMed: 26400949]

Sykora P, Misiak M, Wang Y, Ghosh S, Leandro GS, Liu D, Tian J, Baptiste BA,Cong WN, Brenerman BM, Fang E, Becker KG, Hamilton RJ, Chigurupati S, Zhang Y, Egan JM, Croteau DL, Wilson DM, 3rd, Mattson MP, Bohr VA, 2015 DNA polymerase β deficiency leads to neurodegeneration and exacerbates Alzheimer disease phenotypes. Nucleic Acids Res. 43, 943–959. [PubMed: 25552414]

Vossel KA, Tartaglia MC, Nygaard HB, Zeman AZ, Miller BL, 2017 Epileptic activity in Alzheimer's disease: causes and clinical relevance. Lancet Neurol. 16, 311–322. [PubMed: 28327340]

Yamamoto K, Tanei Z, Hashimoto T, Wakabayashi T, Okuno H, Naka Y, Yizhar O, Fenno LE, Fukayama M, Bito H, Cirrito JR, Holtzman DM, Deisseroth K, Iwatsubo T, 2015 Chronic optogenetic activation augments aβ pathology in a mouse model of Alzheimer disease. Cell Rep. 11, 859–865. [PubMed: 25937280]

Zamboni G, Huey ED, Krueger F, Nichelli PF, Grafman J, 2008 Apathy and disinhibition in frontotemporal dementia: insights into their neural correlates. Neurology 71, 736–742. [PubMed: 18765649]

Zang Y, Jiang T, Lu Y, He Y, Tian L, 2004 Regional homogeneity approach to fMRI data analysis. Neuroimage 22, 394–400. [PubMed: 15110032]

Zempel H, Thies E, Mandelkow E, Mandelkow EM, 2010 Abeta oligomers cause localized Ca(2+) elevation, missorting of endogenous Tau into dendrites, Tau phosphorylation, and destruction of microtubules and spines. J. Neurosci 30, 11938–11950. [PubMed: 20826658]

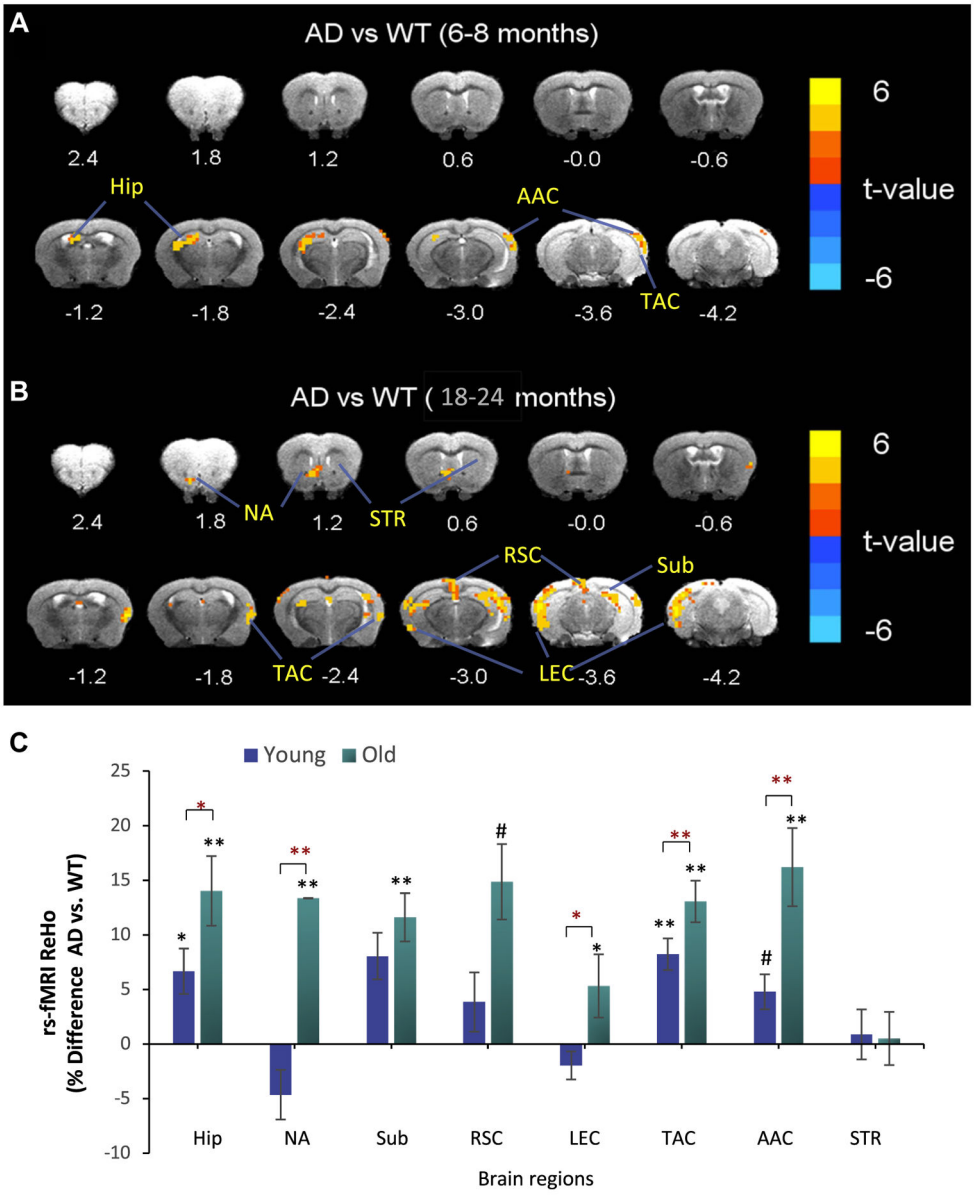

Fig. 1.

Brain regional resting state functional magnetic resonance imaging analysis reveals age-related increases in ReHo in Hip and functionally associated cerebral cortical regions in 3 × TgAD mice. ReHo analysis was performed on young and old 3 × TgAD (AD) and WT mice. (A and B) Images showing ReHo in AD versus WT mice at young (A; 6–8 months of age) and old (B; 18–24 months) ages. Brain topography revealed regions with elevated ReHo (t-values) in AD versus WT mice (n = 8–10 mice/group). (C) Regional ReHo data are expressed as percentage difference in ReHo values of 3 TgAD mice compared to WT mice. Values are the mean and standard error of the mean. $^{\#}p < 0.05$, AD versus WT (asterisk); $p < 0.01$, AD versus WT (double asterisk); $^{\#}p < 0.05$, young versus old (red asterisk); $p < 0.01$, young versus old (red double asterisk). Abbreviations: AAC, auditory association cortex; AD, Alzheimer's disease; EC, entorhinal cortex; Hip, hippocampus; NA, nucleus

accumbens; ReHo, regional homogeneity; RSC, retrosplenial cortex; Sub, subiculum; STR, striatum; TAC, temporal association cortex; WT, wild type. (For interpretation of the references to color in this figure legend, the reader is referred to the Web version of this article.)

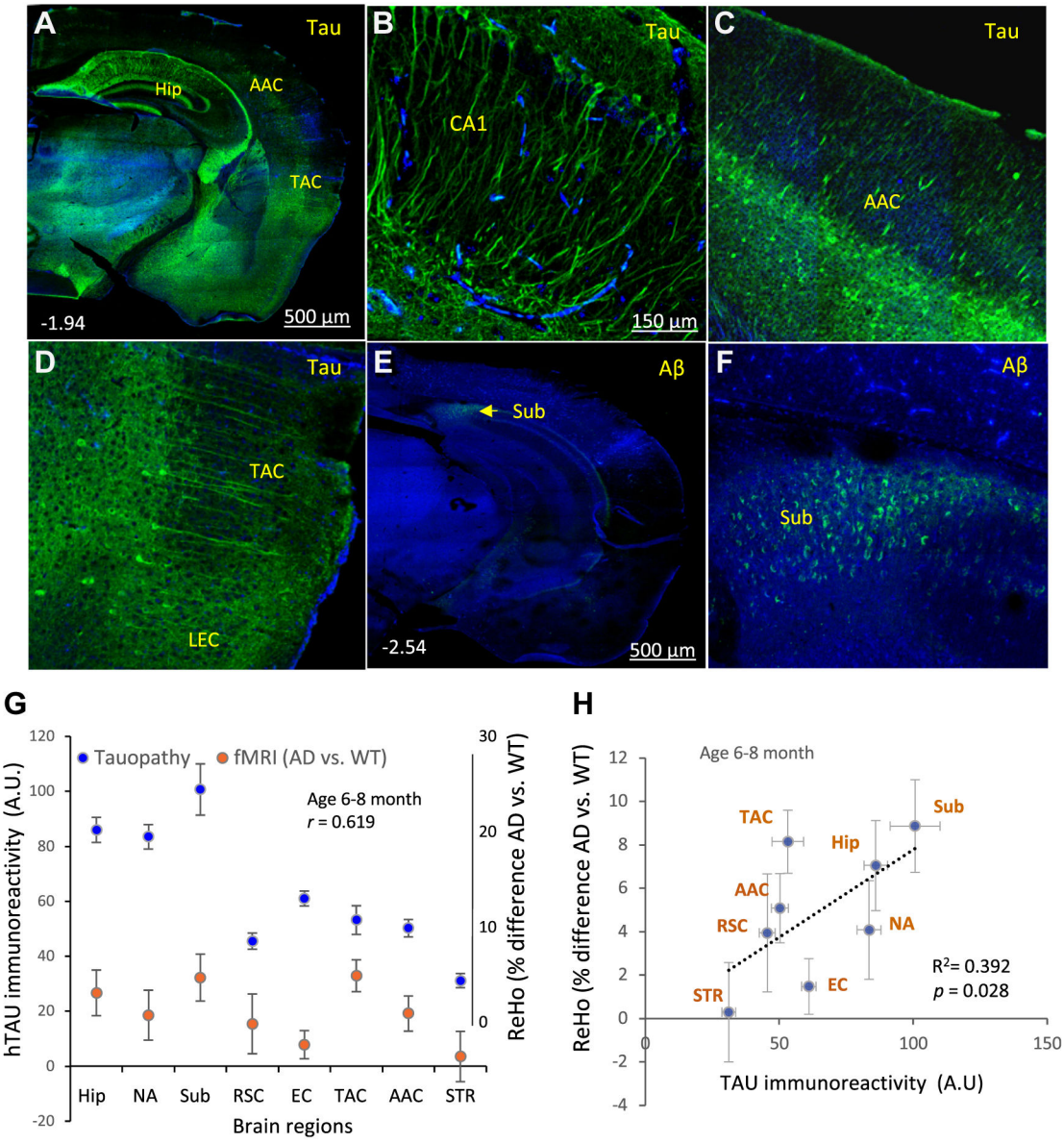

Fig. 2.

ReHo is correlated with tau pathology in the brains of 6- to 8-month-old 3 × TgAD mice. (A–D) Coronal brain sections from 6- to 8-month-old 3 × TgAD mice were immunostained with an antibody against human Tau (hTau). The low-magnification image in panel A reveals prominent hTau accumulation in neurons in the Hip and adjacent regions of the cerebral cortex. The higher magnification images show hTau immunoreactivity in the dendrites and cell bodies of hippocampal CA1 pyramidal neurons (B), layer V neurons in the AAC (C) and LEC (D). (E and F) Coronal brain sections from 6- to 8-month-old 3 × TgAD mice were immunostained with an antibody against Aβ. The low-magnification image in panel D reveals lack of Aβ in all brain regions except the subiculum. The higher magnification image shows intracellular Aβ in neurons in the Sub (F). These images are representative of brains from eight 3 × TgAD mice. (G) Quantitative analyses of group mean of hTau

immunoreactivity and ReHo value (% difference AD vs. WT) in the indicated brain regions. (H) Linear regression analysis of brain regional ReHo value (% difference AD vs. WT), plotted against relative tau immunoreactivity level from the same group of AD mice (correlation coefficient $r = 0.619$; $n = 8$ mice/per group). Abbreviations: AAC, auditory association cortex; AD, Alzheimer's disease; Aβ, amyloid β peptide; EC, entorhinal cortex; Hip, hippocampus; LEC, lateral entorhinal cortex; NA, nucleus accumbens; ReHo, regional homogeneity; RSC, retrosplenial cortex; STR, striatum; Sub, subiculum; TAC, temporal association cortex; WT, wild type.

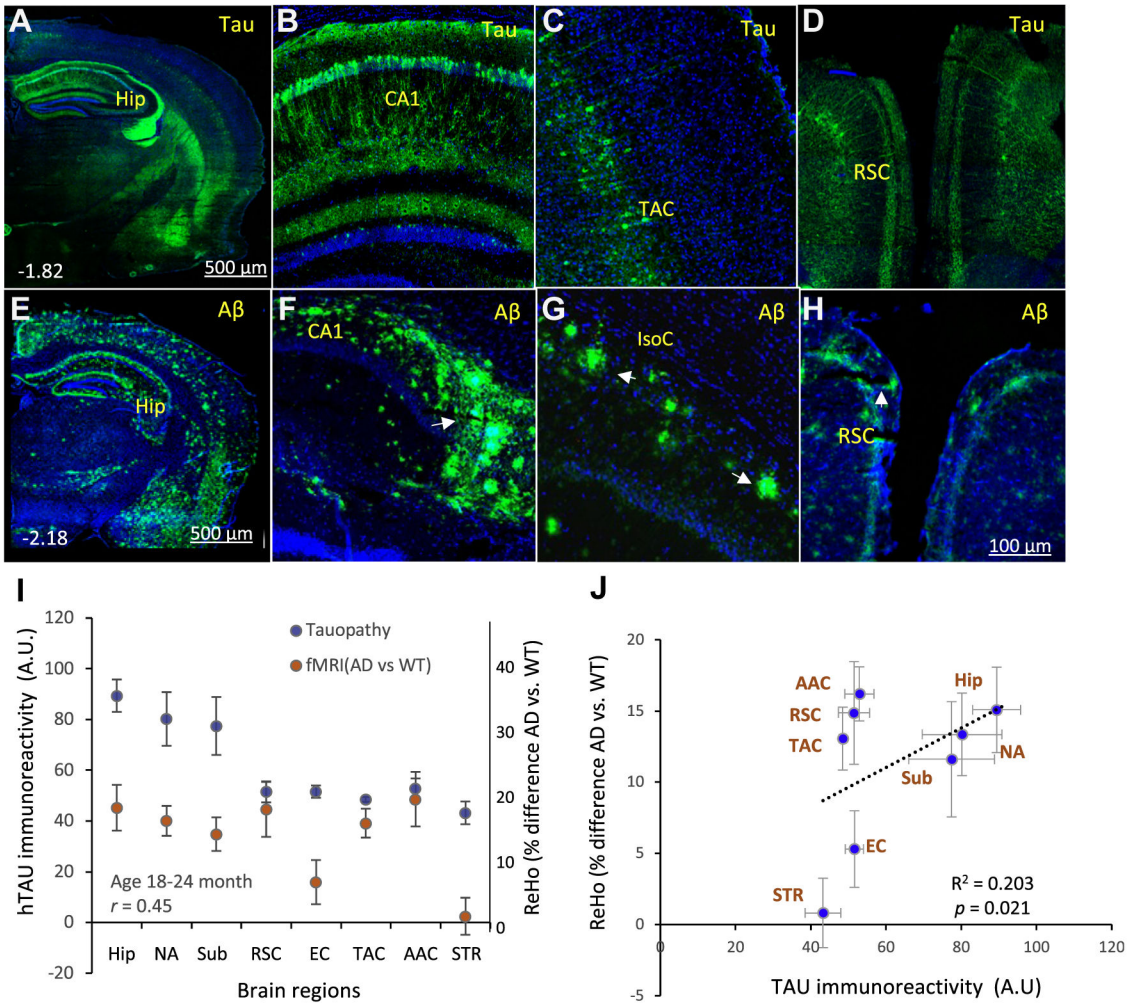

Fig. 3.

Elevated ReHo is correlated with tau pathology in the brains of 18- to 24-month-old 3 × TgAD mice. (A–D) Coronal brain sections from 18- to 24-month-old 3 × TgAD mice were immunostained with an antibody against hTau. The low-magnification image in panel A reveals prominent hTau accumulation in neurons in the Hip, as well as in the TAC and RSC. The higher magnification images show hTau immunoreactivity in the dendrites and cell bodies of hippocampal CA1 pyramidal neurons (B); layer V neurons in the TAC (C) and neurons in the RSC (D). (E–H) Coronal brain sections from 18- to 24-month-old 3 × TgAD mice were immunostained with an antibody against Aβ. The low-magnification image in panel E reveals Aβ deposits in the pyramidal cell layers and dentate gyrus of the Hip in the overlying cerebral cortex and in the EC. The higher magnification images show Aβ deposits in CA1 and CA3 regions of the Hip (F); isocortex (IsoC; G); and RSC (H). These images are representative of brains from ten 3 × TgAD mice. (I) Results of quantitative analyses of associations between group mean of hTau immunoreactivityand ReHo value in the indicated brain regions (% difference AD vs. WT; correlation coefficient $r = 0.45$; $n = 8$ mice/per group). (J) Linear regression analysis of brain regional ReHo value differences between WT

and AD mice, plotted against relative tau immunoreactivity level. The arrow in panel (F) points to amyloid plaques in the subiculum. Abbreviations: AAC, auditoryassociation cortex; AD, Alzheimer's disease; Aβ, amyloid β-peptide; EC, entorhinal cortex; Hip, hippocampus; IsoC, isocortex; NA, nucleus accumbens; ReHo, regional homogeneity; RSC, retrosplenial cortex; STR, striatum; Sub, subiculum; TAC, temporal association cortex; WT, wild type.

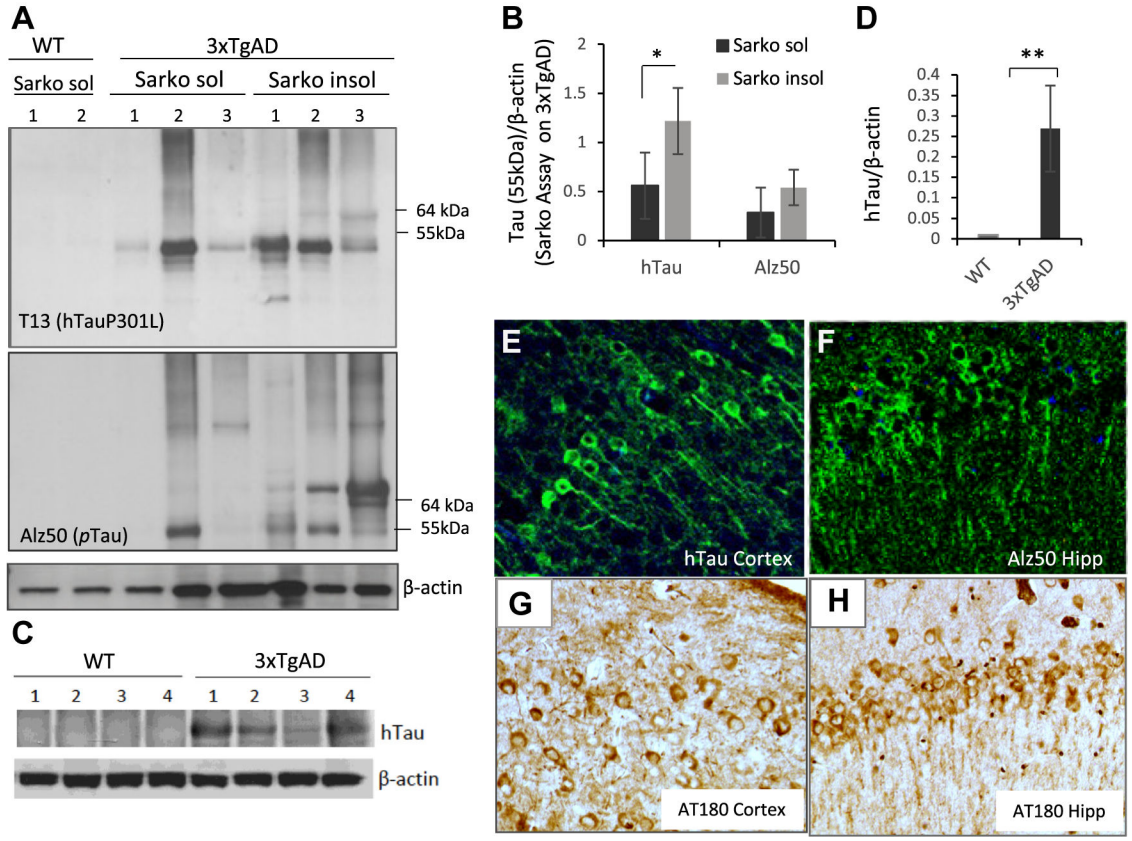

Fig. 4.

Characterization of tauopathy in 3 × TgAD mice. (A) Immunoblots of cerebral cortex tissue samples from 1-year-old WT and 3 × TgAD mice. Blots of samples from the sarkosyl-soluble or -insoluble fractions were probed with antibodies against mutant human tau (upper blot; 55 kDa band), phospho-tau (Alz50 antibody) (middle blot), and β-actin (lower blot). The band at 55 kDa corresponding to human tau was quantificated. (B) Results of quantification of sarkosyl-soluble and -insoluble hTau in cerebral cortex tissue samples from 1-year-old 3 × TgAD mice. *$p < 0.05$. (C) hTau protein immunoreactivity is not detectable in cerebral cortex tissue from WT mice by standard Western blot with anti-hTau antibody. (D) Results of quantification of mutant hTau levels in cerebral cortex tissues from WT and 3 × TgAD mice. **$p < 0.001$. (E–H) Images showing immunoreactivity of neurons with the human tau antibody and phospho-tau antibody Alz50 and AT180 in the Hip and cerebral cortex of a 1-year-old 3 × TgAD mouse. Abbreviations: AD, Alzheimer's disease; Hip, hippocampus; WT, wild type.